ISSN: 2639-0108

Research Article

Advances in Theoretical & Computational Physics

Raman Activity of HS-(CH_2) –NH-Coumarin Molecule Adsorbed on the Surface of Gold Nanostructures with various Morphologies

Sanele Nyembe[1,2], Poslet Shumbula[3], Nosipho Moloto[2], Gebhu Ndlovu[1], Nikiwe Mhlanga[1], Lucky Sikhwivhilu[1*]

[1]*DST/Mintek Nanotechnology Innovation Centre, Advanced Materials Division, Mintek, Private Bag X3015, Randburg, Johannesburg 2125, South Africa*

[2]*Molecular Science Institute, School of Chemistry, University of the Witwatersrand, Private Bag 3, Wits 2050, South Africa*

[3]*Department of Chemistry, University of Limpopo, Private Bag X1106 Sovenga, 0727, South Africa*

[*]Corresponding author

Lucky Sikhwivhilu, DST/Mintek Nanotechnology Innovation Centre, Advanced Materials Division, Mintek, Private Bag X3015, Randburg, Johannesburg 2125, South Africa.

Submitted: 27 Aug 2021; **Accepted:** 30 Aug 2021; **Published:** 06 Sep 2021

Citation: *Sanele Nyembe, Poslet Shumbula, Nosipho Moloto, Gebhu Ndlovu, Nikiwe Mhlanga, Lucky Sikhwivhilu. (2021). Raman Activity of HS-(CH_2) –NH-Coumarin Molecule Adsorbed on the Surface of Gold Nanostructures with various Morphologies. Adv Theo Comp Phy, 4(3), 259-265.*

Abstract

Synthesis of gold nanowires with an average diameter of 10 nm and length of up to 20 µm was achieved through a three-step heterogeneous nucleation process. Gold nanowires were formed through coalescence of spherical nanocrystals leading to grain growth and subsequently uneven nanowires. Furthermore, the uneven gold nanowires experienced thinning driven by thermodynamics to form relatively even nanowires with smaller diameters. Gold nanowires showed enhanced Raman activity in respect to enhancement factor than respective spherical gold nanoparticles with average particle sizes of 14 nm, 30 nm and 40 nm. The better Raman activity of gold nanowires with respect to spherical morphology was attributed to how they adsorb Raman active molecules, which are surface adsorption and network entanglement.

Keywords: Gold Nanowires, Surface-Enhanced Raman Spectroscopy, Transmission Electron Microscope (TEM), Enhancement Factor (EF), Raman Active Compound, Alkanethiol-Coumarin

Introduction

Physical properties of metal nanostructures and their applications are generally influenced by their size and shape [1-2], which have attracted a lot of attention in the field of science [3]. However, in recent years, the attention has been focused on the study of one-dimensional metal nanowires especially gold and silver for their application in Surface-Enhanced Raman Spectroscopy (SERS). Z. Huang et al reported that silver (Ag) exhibits the highest SERS activity than other metals [4-7]. Even though gold exhibit relatively poor SERS activity than silver, however, gold properties such as better biocompatibility and high chemical stability in aqueous medium makes it more suitable for SERS application [8]. Gold nanowires with high aspect ratio are ideal for adsorption of Raman active compounds in SERS applications of high adsorption sites via gold multifaceted nature and high surface area to volume ratio [1-3]. Although anisotropic gold nanostructures can be easily controlled and synthesized with some level of precision the understanding of the growth mechanism, especially that of ultrathin nanowires, remains enigmatic [9-10]. The current methods of synthesizing ultrathin gold nanowires utilises high temperatures, which is economically unfavourable [10-11]. Therefore, there is still a need to improve the production and also quality of ultrathin gold nanowires and understanding their growth mechanism.

SERS is a surface technique that provides high Raman scattering enhancement of molecules adsorbed on a rough metal surface [12-14]. There are currently two well-known theories detailing the mechanism of SERS amplification, which are (i) electromagnetic enhancement and (ii) chemical enhancement [12-14]. The electromagnetic enhancement increases the Raman scattering when surface Plasmon is excited which leads to amplification of the electromagnetic field of the metal surface [14]. However, chemical enhancement occurs when the chemical molecules get adsorbed onto the metal surface leading to change in the polarizability [13-14]. SERS is a non-destructive technique with relatively low detection limits and high sensitivity and it requires a simple sample preparation.

In this study, a new perspective to an old method of synthesizing ultrathin gold nanowires will be described and a potential growth

mechanism will be proposed. To the best of our knowledge the use of this exact modified chemical route for the synthesis of ultrathin gold nanowires has not been previously reported. Furthermore, the ultrathin gold nanowires will be used for SERS applications using HS-(CH_2) -NHCO-coumarin as a Raman active molecule. The calculated enhancement factor (EF) of ultrathin gold nanowires will be compared with that of synthesized spherical gold nanoparticles with average sizes of 14, 30 and 40 nm and those nanowires reported in literature.

Experimental

Materials

Cetyltrimethylammonium bromide (CTAB, 99% purity), Hydrogen tetrachloroaurate (III) tri-hydrate ($HAuCl_4.3H_2O$, >99.9% purity), L-Ascorbic acid (>99% purity), trisodium citrate dehydrate (>99% purity), sodium borohydride ($NaBH_4$, 99% purity) and HS-(CH_2) -NHCO-coumarin alkanethiol were all used as purchased from Sigma Aldrich, (RSA) and were used without further purification. Silver nitrate ($AgNO_3$, 99% purity) was used as purchased from Fluka (RSA). Deionised water was used to prepare all the solutions.

Preparation of Gold Seeds and Growth Solution

The CTAB stabilised seeds were prepared by mixing $HAuCl_4.3H_2O$ (0.25 mM) and CTAB (75 mM) in a beaker under constant stirring (800rpm) at room temperature. Then ice-cold $NaBH_4$ (0.6mM) was added to the mixture and the colour changed from colourless to purple. These seeds were stored in a dark cupboard for at least 2 hours before use.

The growth solution was prepared by mixing CTAB (25 mM), $HAuCl_4.3H_2O$ (0.25 mM), $AgNO_3$ (100 mM) and L-ascorbic acid (0.032 ml of 100 mM) in a 10 ml vial. The mixture was gently hand-shaken for 3 minutes to ensure homogeneity. The growth solution was prepared at room temperature and was used immediately for the growth of gold nanowires.

Synthesis of Spherical Gold Nanoparticles

Spherical AuNPs were prepared through an in-situ nucleation method. The weight % (wt/wt %) of tri-sodium citrate to tetrachloroaurate that were used were from 0.7, 0.5 and 0.2. The mixtures were then allowed to boil for five minutes under constant stirring then cooled to room temperature. The final mixtures were left in a dark cupboard for at least 24 hours before characterisation.

Synthesis of Ultrathin Gold Nanowires

Gold nanowires were grown by mixing 1 ml of the seed solution and 4 ml of the growth solution in a 10 ml vial. The mixture was gently stirred for 5 minutes and then stored in a dark cupboard for 48 hours before analysis. Characterisation of the samples was done using UV-Vis absorption spectra (Lambda 35), High resolution transmission electron microscope (HRTEM, JEM-2100F - 200 kV) and X-Ray Diffraction (Bruker, D8 Advanced equipped with Lynx-eye XE detector.

Surface-Enhanced Raman Spectroscopy Sample Preparation and Characterisation

Raman active alkanethiol (HS-(CH_2) -NHCO-coumarin) was used for surface enhancement Raman spectroscopy on Raman active compound adsorbed on gold nanostructure with various morphologies. A mass of 0.02 mg of HS-(CH_2) -NHCO-coumarin was dissolved in deionised water before mixed with a mass of 1.98 mg of HS-PEG-$(CH_2)_{11}$COOH to make a 1% alkanethiol solution. The four solutions of gold nanostructures were all filtered with a microporous filter. A volume of 10 mL of the filtered gold nanostructures was mixed with 200 µL of 1% alkanethiol solution for co-stabilisation of the gold nanostructures. Furthermore, the four solutions were stirred at room temperature for at least 3 hours to form a homogenous mixture.

The Raman spectroscope that was used was Perkin Elmer Raman Station 400 with the following specifications; wavelength = 785 nm, Focal length = 750 µm, laser spot area = 2540 µm. The Raman was operated with the following settings; 70% laser power from a Raman shift range of 3000 to 100 cm^{-1}, 6 accumulations and an exposure of 3 seconds.

Results and Discussion

Synthesis of Spherical Gold Nanoparticles

Figure 1 showed UV-Vis of samples with 0.2, 0.5 and 0.7 % of citrate salt to gold salt. The UV-Vis spectra showed a monomodal peak for all the samples at wavelengths of 520 nm (0.2%), 517 nm (0.5%) and 514 nm (0.7%). The presence of UV-Vis monomodal peak suggests monodispersed nanomaterials which show that the presence of citrate moiety led to a monodispersed nanoparticle. The wavelength at which the peaks appear is a typical Surface Plasmon Resonance (SPR) band resulting in the formation of gold particles in solution. The position width and intensity of SPR band are dependent on particle size, shape, concentration, and surface-charge, refractive index of the medium and inter-particle interactions. The SPR wavelength decreased with an increase in citrate percentage (Blue-shift) and this is thought to be due to a reduction in particle size.

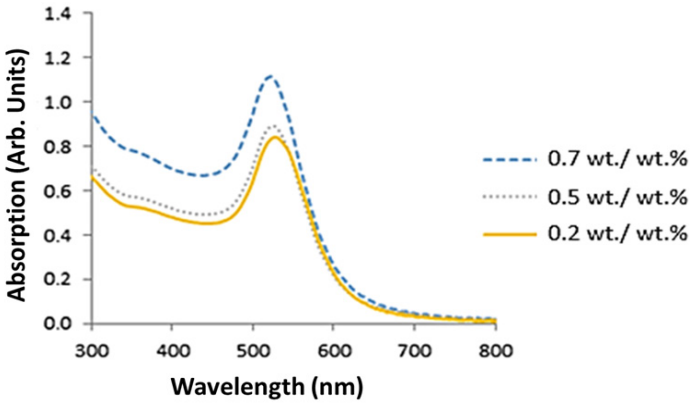

Figure 1: UV-Vis spectra of gold nanoparticles with 0.2, 0.5 and 0.7 weight percentages.

AuNPs were synthesized by classic citrate (Turkevich et al) method with varying citrate/gold salt ratios [15]. Figure 2 showed TEM images of gold nanoparticles containing (a) 0.7 (b) 0.5 and (c) 0.2 % of citrate salt/gold salt ratios with corresponding size distribution histograms with a Gaussian curve fitted into the data, respectively. TEM images show that 0.7, 0.5 and 0.2% samples are made up of nanoparticles with average diameters of 14, 30 and 40 nm. AuNP size increased with a reduction in citrate concentration weight from 0.7 to 0.2 %. The gold nanoparticles were

monodispersed which is in agreement with the UV-Vis single peak observed for all the samples.

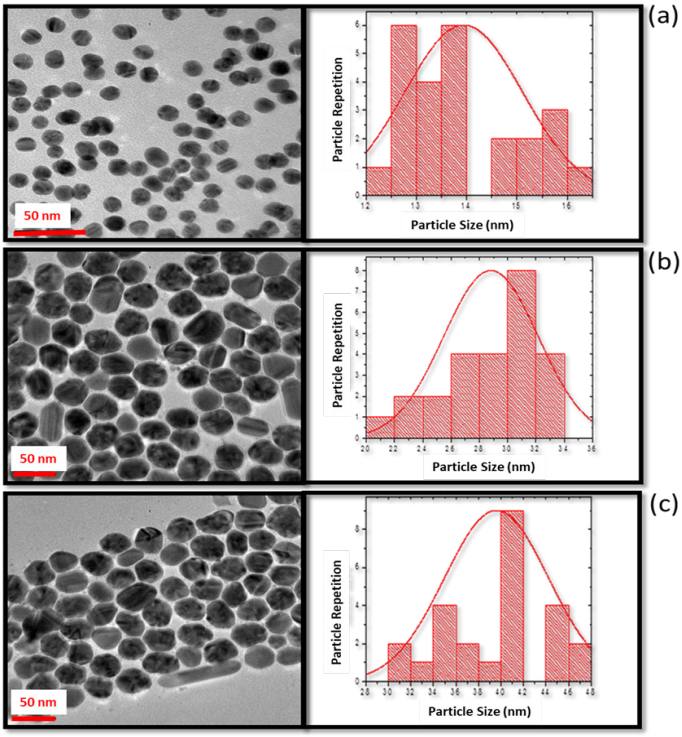

Figure 2: TEM images and size distribution histograms of gold nanoparticles prepared with (a) 0.7, (b) 0.5 and (c) 0.2 citrate salt/gold salt %.

EDX analysis of AuNPs sample with 0.2% (wt/wt) shown in Figure 3 confirmed that the particles were those of gold. EDX spectrum of 0.2% sample was similar to those of 0.5 and 0.7 % samples (not shown). The carbon emanated from the carbon coating done in sample preparation. The EDX results are in agreement with the SPR band position which confirmed the presence of gold nanoparticles.

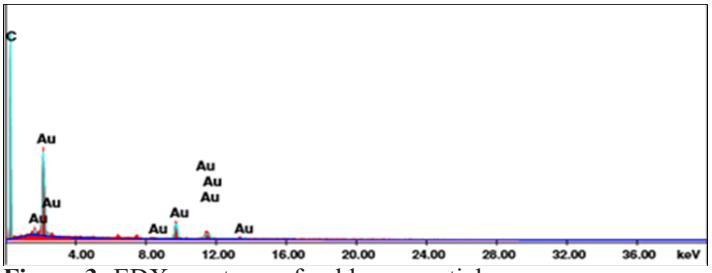

Figure 3: EDX spectrum of gold nanoparticles.

The SEM and UV-Vis results clearly show that a high concentration of citrate led to the formation of small gold nanoparticles (14nm). As the citrate concentration was systematically reduced from 0.7 to 0.2 wt%, the size of the nanoparticles increased to 30 nm then to 40 nm. This change in citrate salt/Au salt influences the pH of the reaction mixture thereby affecting the formation of gold nanoparticles. Furthermore, the increase in the concentration of gold salt might have resulted in increased ionic strength emanating from a high concentration of Au salt which could have a direct impact on both the size and size distribution of the gold nanoparticles. However, when the concentration of citrate was reduced to 0.2 %, steric hindrance was reduced as a result of steric effect leading to particle growth. A balance of citrate molecules and Au^{3+} ions is crucial for controlling the size of gold nanocrystals. The citrate molecules get attached to crystal planes thus hindering growth leading to a formation of specific particle size [15].

Synthesis of Ultrathin Gold Nanowires

Figure 4 showed XRD spectrum of the sample prepared from gold seed and growth solution. The XRD pattern showed the presence of sharp and narrow peaks suggesting a crystalline material. The peaks at 2-theta angles of 25˚[001], 38˚[111], 45˚[200] and 54˚[110] were all indexed to gold, suggesting that gold material produced was phase pure. The X-ray diffraction patterns were collected using a D8 Advance diffractometer equipped with Lynx-eye XE detector operated at 2θ angles between 5 and 80° using a Cobalt X-ray source radiation. Phase identification was accomplished by comparison of measured spectra with the spectra of pure samples from the database (JCPDS, Card No. 4-784).

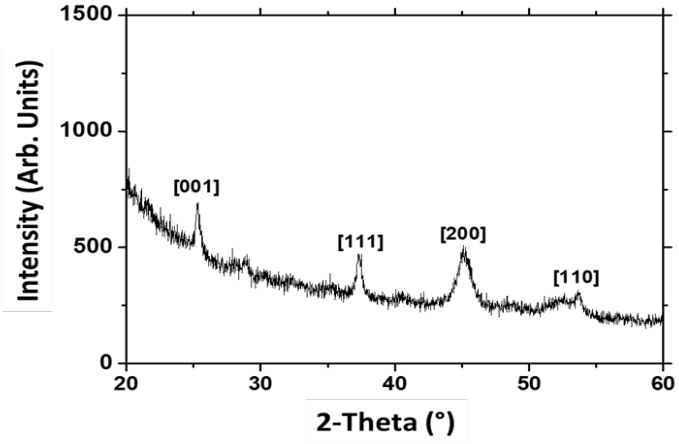

Figure 4: X-Ray diffraction spectrum of gold nanostructures.

Figure 5 showed a TEM image of nanostructures with a nanowire morphology and the EDX spectrum showed that they were made up of gold, which confirms the XRD results. The Cu, Fe, Cr and C from the EDX spectrum all emanated from TEM sample holder and carbon coated copper grid. Gold nanowires had an average diameter of 10 nm with a size distribution of 3 to 12 nm and an average length of up to 20 µm. Thus, the nanowires showed a relatively high aspect ratio of 2000. The TEM image also revealed that the gold nanowires with diameters above 10 nm contained knot like structures.

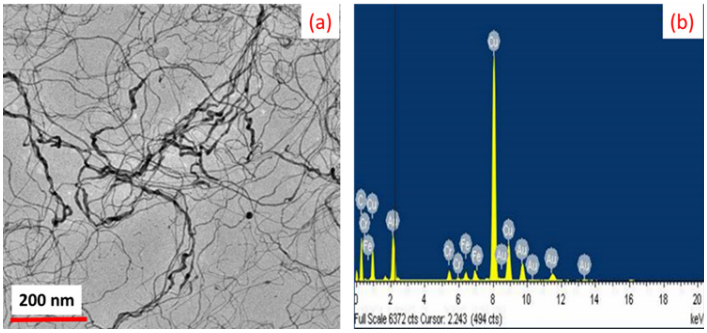

Figure 5: The (a) TEM image of the gold nanowires and respective (b) EDX spectrum.

Mechanism of Formation of Ultrathin Gold Nanowires

The mechanism of formation of the gold nanowires was achieved by sampling aliquots of reacting mixture at different time intervals. Aliquots of the reaction solution were taken over a period of 48 hours (2880 minutes) at time intervals of 30, 120, 240, 480, 1440 and 2880 minutes. The TEM images of the samples taken at different time intervals are shown in Figure 6. The TEM image of the aliquot taken after 30 minutes (Figure 6a) showed spherical gold nanoparticles with an average diameter of 10 nm (range 8-12). This indicates a rapid reduction of Au^{3+} ions from $HAuCl_4$ salt by $NaBH_4$ reducing agent forming CTAB stabilised spherical gold nanoparticles. The TEM image of the aliquot sample taken after 120 minutes (Figure 6b) showed gold nanoparticles that were agglomerated with various shapes but mostly spherical. Some of the gold nanoparticles were found to have coalesced forming relatively bigger gold nanoparticles due to Oswald ripening. Oswald ripening phenomenon is common when the metal nanoparticles are stabilised by CTAB and often led to particle growth [16]. Figure 6 (c) showed the TEM image of the aliquot sample taken after 240 minutes and it showed a mixture of spherical gold nanoparticles and gold nanowires. The gold nanowires appeared to have formed via coalescence/orientated attachment of spherical nanoparticles, as their surfaces were rough and "chain-like" and their links resembled spherical gold nanoparticles (shown in the Figure 6 (a). The TEM image of the aliquot sample taken after 480 minutes (Figure 6d) showed chain-like gold nanowires, suggesting that the gold nanoparticles underwent an oriented attachment process for form gold nanowires. Oriented attachment crystal growth mechanism requires that primary particles irreversibly fuse together to form secondary monocrystalline particles, which could be driven by van der Waals forces, electrostatic forces, dipole-dipole interaction [17-18], etc. The resulting irregular chain-like structure has a convex and concave region which has high chemical potentials and renders it a thermodynamically unstable structure [19-21]. This thermodynamically driven instability of chain-like gold nanowires led to thinning of the nanowires forming small nanowires in-terms of their diameter, which is observed in the TEM image shown in Figure 6 (e). Since the primary spherical gold nanoparticles were of various sizes, the chain-like structures extended into thinner nanowires at different rates because of the different chemical potential possessed by each nanowire. It is for this reason that some gold nanowires were found to be thin while others still displayed a chain-like structure after 1440 minutes as shown in the TEM image in Figure 6(e). TEM image in Figure 6(f) showed aliquot taken after 2880 minutes (48 hours) and also showed relatively thinner gold nanowires. These relatively thinner gold nanowires were formed due to extended thinning of the initial chain-like gold nanowires. As a thermodynamically driven process the thinning process was found to be independent of gold nanoparticle (seed) diameter. Interestingly, there are no reports in the literature where gold nanowires were grown in the presence of CTAB as a stabilizer suggesting that this could have played an important role in the thinning and elongation process leading to very long nanowires (up to 20 µm in length)

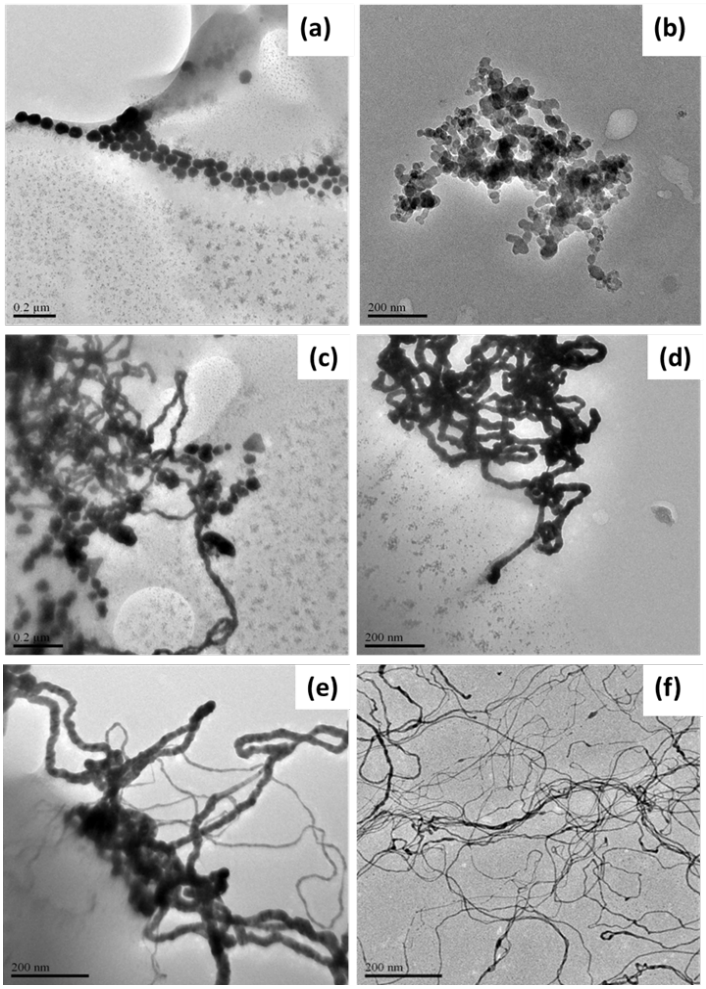

Figure 6: TEM images of gold nanostructures from aliquots taken after (a) 30 min., (b) 120 min., (c) 240 min., (d) 480 min., (e) 1440 min., and (f) 2880 min. of the synthesis reaction time.

Surface-Enhanced Raman Spectroscopy

Figure 7 showed the (a) chemical structure and the (b) Raman spectrum of HS-$(CH_2)_{11}$-NHCO-coumarin molecule. The chemical structure of HS-$(CH_2)_{11}$-NHCO-coumarin molecule contained C=O, C-C, C-OH, C=C, S-H and N-H functional groups. Figure 7 (b) showed the Raman spectrum of HS-$(CH_2)_{11}$-NHCO-coumarin molecule, and there were peaks at 2700 cm^{-1} (S-H), 1700 cm-1 (C=S), 1665 cm^{-1} (C=O) and weak aliphatic C-C bond peak at 1100 cm^{-1}. The HS-$(CH_2)_{11}$-NHCO-coumarin molecule interacts with the surface of the gold surface via the thiol group (H-S), which is broken to form a new Au-S bond [22-23].

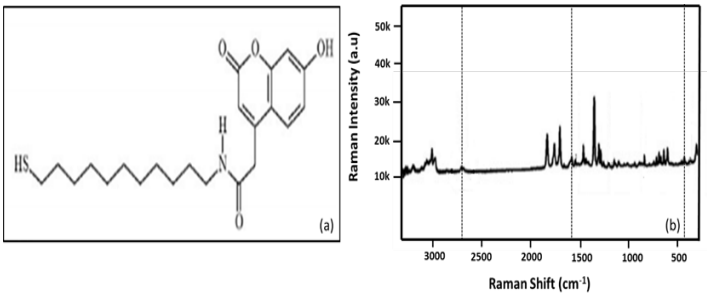

Figure 7: The (a) chemical structure and (b) Raman spectrum of HS-(CH2)11-NHCO-coumarin molecule.

Figure 8 showed Raman spectra of HS-$(CH_2)_{11}$-NHCO-coumarin and (a) Au_{14nm}-S-$(CH_2)_{11}$-NHCO-coumarin, (b) Au_{30nm}-S-$(CH_2)_{11}$-NHCO-coumarin and (c) Au_{40nm}-S-$(CH_2)_{11}$-NHCO-coumarin and (d) Au nanowires-S-$(CH_2)_{11}$-NHCO-coumarin. The Raman analysis was carried out to study the interaction between HS-$(CH_2)_{11}$-NHCO-coumarin molecule and the surface of gold nanostructures with different morphologies. The spectrum of Au-S-$(CH_2)_{11}$-NHCO-coumarin (Figure 7. a) showed that the thiol peak at 2700 cm^{-1} disappeared which was attributed to the new Au-S bond formation of the HS-$(CH_2)_{11}$-NHCO-coumarin with the surface of gold nanoparticles. This caused a new vibrational peak to appear at 400 cm-1 which was associated with Au-S vibration. The intensity of the Au-S peak at a Raman shift of 400 cm-1 was important for the calculation of enhancement factor. The interaction of HS-(CH2)11-NHCO-coumarin with the gold nanostructures showed a strong electromagnetic effect assigned to the CH_2 asymmetric vibrations observed at 1600 cm-1. The other important peak intensity enhancement was observed at a region of 800-950 cm-1 that was due to aliphatic C-C vibrations [23]. The spectra of Au-S-$(CH_2)_{11}$-NHCO-coumarin molecule and all the gold

nanostructures with different morphologies were similar in peak positions. However, the Au-S peak intensity at a Raman shift of 400 cm-1 was different for various gold nanostructures, suggesting that the enhancement factors were not the same. The Au-S peak intensity increased from Au (14nm) to Au (30nm) samples and then decreased for Au (40nm) sample. The Au-S peak intensity for Au (nanowires) was the highest for all gold nanostructures as shown in Figure 8. The peak intensity of coumarin on gold nanowires was found to be the highest of all the nanostructures.

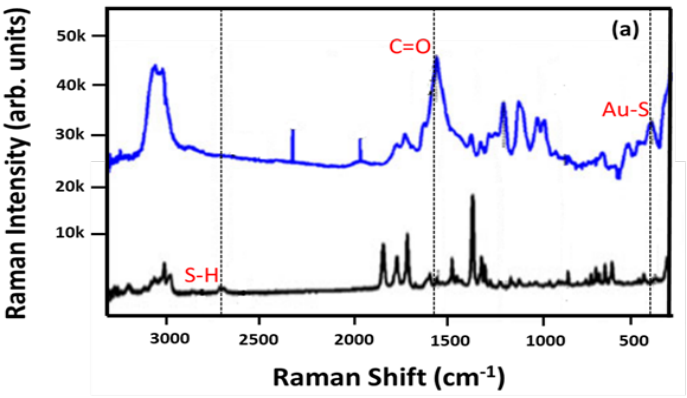

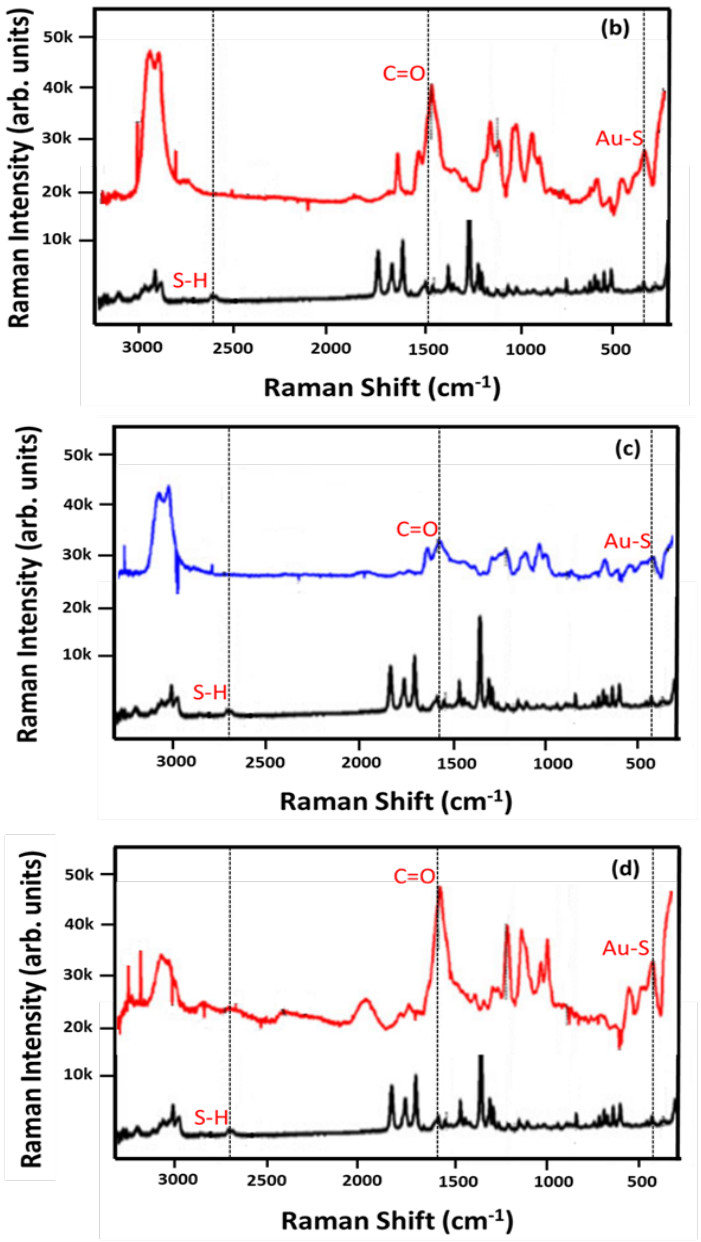

Figure 8: The Raman spectra of HS-$(CH_2)_{11}$-NHCO-coumarin adsorbed on spherical gold nanoparticles with average sizes of (a) 14nm, (b) 30 nm (c) 40 nm. HS-$(CH_2)_{11}$-NHCO-coumarin adsorbed on gold nanowires is shown in (d).

The SERS enhancement factor is a noble indicator of the adsorption of Raman active compound (HS-(CH2)11-NHCO-coumarin) to the surface of gold nanoparticles and indicator of SERS sensitivity. The enhancement factor was calculated using Equation 1.

$$EF = \left(\frac{I_{surf}}{I_{bulk}}\right) * \left(\frac{N_{bulk}}{N_{surf}}\right) \quad (1)$$

Where I_{surf} and I_{bulk} are the intensities of the vibrational mode in the SERS and the vibrational mode in the Raman spectrum. Nbulk and N_{surf} are the number of free HS-$(CH_2)_{11}$-NHCO-coumarin and Au-HS-(CH_2)11-NHCO-coumarin. N_{bulk} and N_{surf} can be calculat-

ed according to Equation 2 and 3, respectively [24].

$$N_{bulk} = Ah\frac{\rho}{m} \quad (2)$$

$$N_{surf} = 4\pi r^2 CAN \quad (3)$$

Where A, h, ρ and m are laser spot area, the focal length, the density of HS-$(CH_2)_{11}$-NHCO-coumarin and it molecular mass (40,55 gmol-1) from equation 2, respectively. In equation 3, r, C, A and N are the average radius of the Au nanoparticles (aspect ratio was used for Au nanowires), surface density of the HS-$(CH_2)_{11}$-NHCO-coumarin, the area of the laser spot and surface coverage of the Au nanostructures (particles μm^{-2}), respectively [24]. Substituting Equation (2) and (3) into Equation (1), the following Equation 4 is obtained;

$$EF = \left(\frac{I_{surf}}{I_{bulk}}\right)\left(\frac{Ah\rho}{4\pi mr^2 CAN}\right) \quad (4)$$

The EF for Au_{14nm}, Au_{30nm}, Au_{40nm}, and $Au_{nanowires}$ were calculated to be 80 000, 140 000, 40 000 and 270 000, respectively The EF was calculated using the enhanced intensities of the asymmetric vibrational bands of CH_2 observed at 1400 cm^{-1} for all the samples. Figure 9 showed the graph of calculated EF values for various gold nanostructures.

When the size of Au nanoparticles was increased from 14 to 30 nm an increase in the EF was observed (80 000 for 14nm and 140 000 for 30 nm) and this was attributed to an increasing contribution of high order Plasmon modes which increases the electromagnetic field in larger particles [25]. The increase in an electromagnetic field led to a higher dipole moment of vibrating molecules of HS-$(CH_2)_{11}$-NHCO-coumarin and caused a higher EF for 30 nm nanoparticles than 14 nm [25]. But the high electromagnetic field observed when the Au nanoparticles increased is accompanied by an increase in scattering efficiency which resulted in lower Raman signal [25]. The negative effect of scattering efficiency is supported by a decrease in EF for Au nanoparticles with the size of 40 nm (40 000). However, the gold nanowires showed the highest EF (270 000) compared to spherical gold nanoparticles with average sizes of 14, 30 and 40 nm. Not only did the nanowires show EF higher than that of nanoparticles but also highest ever reported for Au nanowires regardless of the method of preparation. This was attributed to the fact that gold nanowires adsorb Raman active compounds via two mechanisms, which are (i) surface adsorption due to the surface reactivity of gold nanowires and (ii) Network entrapping through their "web" network [26]. In this study, the gold nanowires had an average diameter of 10 nm hence they have a relatively high surface area which is important for increasing adsorption capacity for Raman active molecules on their surface. The high aspect ratio, chemical stabilizers used, and stability of the nanowires are all considered important contributing factors for higher EF. Poor nanowire stability is one of the reasons why nanowires with a diameter above 35 nm are typically preferred for SERS activity [28]. The same is true for nanoparticles (gold and silver) with dimeter range of 2-50 nm as they tend to possess high surface energies. This often requires the use of stabilizers that could reduce aggregation as a way to maintain a high unit surface area [27, 28]. The Au nanowires shown in Figure 5 (a) shows that they formed a spider web-like network with interstices smaller than 1 nm. These interstices have been reported to be responsible for further entrapment of HS-(CH_2)11-NHCO-coumarin molecules [11]. The spider web-like network was exclusively found in gold nanowires and not in the spherical gold nanoparticles. Hence, gold nanowires were found to have a relatively high EF value compared to spherical nanoparticles.

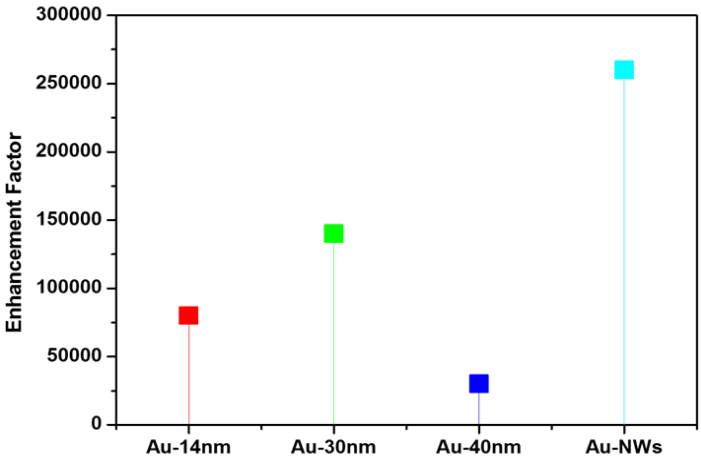

Figure 9: Line graph correlating the calculated enhancement factor values for gold nanostructures with different morphologies.

Conclusion

Gold nanowires with average diameter of 10 nm and length of up to 20 µm were successfully synthesised via thinning mechanism. This was done using a uniquely modified synthesis method. The Au nanoparticles were initially spherical nanowires that experienced coalescence due to a limited stabilising agent to form relatively bigger nanowires, which thinned to form narrow size nanowires. The Au nanowires Raman activity was compared to spherical gold nanoparticles that were synthesized using the Turkevich method. The calculated enhancement factor showed that Au nanowires were better in SERS application than all the tested gold nanoparticles with various sizes (i.e. 14, 30 and 40 nm). Furthermore, the nanowires produced using a modified method gave the highest EF ever recorded in the literature for Au nanowires. This was partly due to the fact that the ultrathin Au nanowires had a better or improved adsorption capacity for Raman active compounds resulting from the surface activity and entrapment via interstices formed by their network, whereas, spherical nanoparticles adsorb them using surface activity only.

Acknowledgments

This work was supported by Mintek, Department of Science and Innovation (DSI) South Africa, through the DSI/Mintek Nanotechnology Innovation Centre (NIC). The authors also acknowledge the University of Witwatersrand for the support. Lastly, the authors wish to acknowledge NIPMO (The National Intellectual Property Management Office - South Africa) for support.

References

1. Khan, I., Saeed, K., & Khan, I. (2019). Nanoparticles: Properties, applications and toxicities. Arabian journal of chemistry, 12(7), 908-931.
2. Ali, A., Hira Zafar, M. Z., ul Haq, I., Phull, A. R., Ali, J. S., & Hussain, A. (2016). Synthesis, characterization, applications, and challenges of iron oxide nanoparticles. Nanotechnology, science and applications, 9, 49-67.

3. Dreaden, E. C., Alkilany, A. M., Huang, X., Murphy, C. J., & El-Sayed, M. A. (2012). The golden age: gold nanoparticles for biomedicine. Chemical Society Reviews, 41(7), 2740-2779.
4. Huang, Z., Li, Z., Chen, R., Chen, G., Lin, D., Xi, G., ... & Lei, J. (2011). The application of silver nanoparticle based SERS in diagnosing thyroid tissue. In Journal of Physics: Conference Series (Vol. 277, No. 1, p. 012014). IOP Publishing.
5. Liu, B. C., & Zou, B. S. (2007). Liu and Zou Reply. Physical Review Letters, 98(3), 039102-039110.
6. Chang, J., Zhang, A., Huang, Z., Chen, Y., Zhang, Q., & Cui, D. (2019). Monodisperse Au@ Ag core-shell nanoprobes with ultrasensitive SERS-activity for rapid identification and Raman imaging of living cancer cells. Talanta, 198, 45-54.
7. Pînzaru, S. C., Andronie, L. M., Domsa, I., Cozar, O., & Astilean, S. (2008). Bridging biomolecules with nanoparticles: surface-enhanced Raman scattering from colon carcinoma and normal tissue. Journal of Raman Spectroscopy: An International Journal for Original Work in all Aspects of Raman Spectroscopy, Including Higher Order Processes, and also Brillouin and Rayleigh Scattering, 39(3), 331-334.
8. Wang, L., Yang, Q., Cui, Y., Gao, D., Kang, J., Sun, H., ... & Chen, S. (2017). Highly stable and biocompatible dendrimer-encapsulated gold nanoparticle catalysts for the reduction of 4-nitrophenol. New Journal of Chemistry, 41(16), 8399-8406.
9. Marks, L. D. (1994). Experimental studies of small particle structures. Reports on progress in physics, 57(6), 603.
10. Hirai, H. (1979). Formation and catalytic functionality of synthetic polymer-noble metal colloid. Journal of Macromolecular Science—Chemistry, 13(5), 633-649.
11. Feng, H., Yang, Y., You, Y., Li, G., Guo, J., Yu, T., ... & Xing, B. (2009). Simple and rapid synthesis of ultrathin gold nanowires, their self-assembly and application in surface-enhanced Raman scattering. Chemical communications, (15), 1984-1986.
12. Uskoković-Marković, S., Jelikić-Stankov, M., Holclajtner-Antunović, I., & Đurđević, P. (2013). Raman spectroscopy as a new biochemical diagnostic tool. Journal of Medical Biochemistry, 32 (2), 96-103.
13. Rodger, C., Rutherford, V., White, P. C., & Smith, W. E. (1998). Towards quantitative surface enhanced resonance Raman scattering (SERRS): a study of aggregation and concentration for two rhodamine dyes. Journal of Raman spectroscopy, 29(7), 601-606.
14. Ang, L. K., Lau, Y. Y., Gilgenbach, R. M., & Spindler, H. L. (1997). Analysis of laser absorption on a rough metal surface. Applied physics letters, 70(6), 696-698.
15. Turkevich, J. and Hillier, J. (1949). Electron Microscopy of Colloidal Systems. Analytical Chemistry, 21(4), 475-485.
16. Nyembe, S., Mpelane, S., Shumbula, P., Harris, R., Moloto, N., & Sikhwivhilu, L. (2015). The Effects of gold seeds stabilizing agent on gold nanostructures morphologies. Materials Today: Proceedings, 2(7), 4149-4157.
17. Lv, W., He, W., Wang, X., Niu, Y., Cao, H., Dickerson, J. H., & Wang, Z. (2014). Understanding the oriented-attachment growth of nanocrystals from an energy point of view: a review. Nanoscale, 6(5), 2531-2547.
18. Zhang, Q., Liu, S. J., & Yu, S. H. (2009). Recent advances in oriented attachment growth and synthesis of functional materials: concept, evidence, mechanism, and future. Journal of Materials Chemistry, 19(2), 191-207.
19. Li, D., Nielsen, M. H., Lee, J. R., Frandsen, C., Banfield, J. F., & De Yoreo, J. J. (2012). Direction-specific interactions control crystal growth by oriented attachment. Science, 336(6084), 1014-1018.
20. Zhang, H., & Banfield, J. F. (2014). Interatomic Coulombic interactions as the driving force for oriented attachment. Cryst EngComm, 16(8), 1568-1578.
21. Lu, L., Kobayashi, A., Kikkawa, Y., Tawa, K., & Ozaki, Y. (2006). Oriented attachment-based assembly of dendritic silver nanostructures at room temperature. The Journal of Physical Chemistry B, 110(46), 23234-23241.
22. Mlambo, M., Mdluli, P. S., Shumbula, P., Skepu, A., Tshikhudo, R., & Moloto, N. (2015). A size-controlled synthesis and characterization of mixed monolayer protected silver-S-(CH_2) 11-NHCO-coumarin nanoparticles and their Raman activities. Journal of materials research, 30(12), 1934-1942.
23. Joo, T. H., Kim, M. S., & Kim, K. (1987). Surface-enhanced Raman scattering of benzenethiol in silver sol. Journal of Raman spectroscopy, 18(1), 57-60.
24. Lin, W. C., Huang, S. H., Chen, C. L., Chen, C. C., Tsai, D. P., & Chiang, H. P. (2010). Controlling SERS intensity by tuning the size and height of a silver nanoparticle array. Applied Physics A, 101(1), 185-189.
25. Xie, Y., Chen, H., Xu, Y., Zhu, L., Ma, H., & Dong, J. W. (2011). An invisibility cloak using silver nanowires. Plasmonics, 6(3), 477-481.
26. Lee, S. J., Morrill, A. R., & Moskovits, M. (2006). Hot spots in silver nanowire bundles for surface-enhanced Raman spectroscopy. Journal of the American Chemical Society, 128(7), 2200-2201.
27. Johnson, L. P., & Matisons, J. G. (2012). Synthesis of high aspect-ratio gold nanowires with highly porous morphology. International Scholarly Research Notices, 2012.
28. Zhang, Y., Chu, W., Foroushani, A. D., Wang, H., Li, D., Liu, J., ... & Yang, W. (2014). New gold nanostructures for sensor applications: a review. Materials, 7(7), 5169-5201.